Advances in Water Resources 142 (2020) 103642

Contents lists available at ScienceDirect

Advances in Water Resources

journal homepage: www.elsevier.com/locate/advwatres

Unsaturated flow in a packing of swelling particles; a grain-scale model

Thomas Sweijen [a,b], S. Majid Hassanizadeh [a,*], Bruno Chareyre [c]

[a] Utrecht University, Department of Earth Sciences, Utrecht, Netherlands
[b] Crux Engineering BV, Amsterdam, Netherlands
[c] University Grenoble Alpes, 3SR, F-38000 Grenoble, France

ARTICLE INFO

Keywords:
Swelling particles
grain-scale model
DEM
Unsaturated flow

ABSTRACT

In this work, a grain-scale modelling technique is introduced for the simulation of unsaturated flow in deforming and swelling granular materials. To do so, a pore-scale model for unsaturated flow is coupled to the discrete element method (DEM). It is assumed that initially a dry packing of particles is quickly invaded by a liquid and becomes fully saturated. Particles start absorbing the liquid and this causes a rearrangement of particles, entrance of air into the packing, and a redistribution of the liquid (i.e. unsaturated flow). Flow was computed using a scheme of implicit pressure solver and explicit saturation update (IMPES), whilst particle movement was modelled using DEM. Simulations are continued until the packing is dry again. This is the first time that such a pore-scale model has been developed. We have used the model to investigate unsaturated flow during drying of a bed of swelling particles. Results indicated that the characteristic time scales of unsaturated flow and water absorption determine the swelling behaviour of the particle packing.

1. Introduction

Unsaturated flow in swelling porous materials poses an intricate and highly coupled problem. Swelling not only causes deformation of the solid phase and rearrangement of grains, but also affects the distribution of the liquid inside the pores, which subsequently affects the swelling of the solid phase. For example, a coal bed may swell due to injection and subsequent adsorption of CO_2 inside the coal matrix, which causes an increase in internal stress and a subsequent decrease in permeability (Espinoz et al., 2014; Pan et al., 2012 and references therein). But, the decrease in permeability inhibits the usage of coal bed for further carbon sequestration. Swelling of porous materials also occurs in anthropogenic materials such hydrophilic binders inside the coating layer of paper during ink injection (see e.g. Lamminmäki et al., 2012), the swelling of potatoes during frying (Takhar, 2014) and the swelling of starch in food (e.g. Tester and Morrison, 1990; Yeh and Li, 1996).

In this work, the focus is on swelling of a bed of Super Absorbent Polymer (SAP) particles, which are used in hygienic products. SAP particles can absorb distilled water up to 1000 times their initial weight and up to 40 times of a fluid having a physiological salinity (e.g. Graham and Wilson, 1998 and references therein). The swelling of an individual SAP particle is a complex process. It includes fluid transport into the polymer framework of particle, ion redistribution inside the polymer framework (Bertrand et al., 2016; Yu et al., 2017; Huyghe and Janssen, 1997), an expanding particle boundary (Radu et al., 2002; Sweijen et al., 2017b), as well as the cracking of surface of an initially dry SAP particle (Ding et al., 2018). The swelling of a bed of SAP particles is not only controlled by the swelling of individual particles, but also by processes occurring within the pores of the particle bed (Diersch et al., 2010; Sweijen et al., 2017a).

Swelling of porous materials is a specific case of hydromechanical coupling that, in general, involves the coupling of deformation of the porous solid and liquid flow inside its pores. To characterize hydromechanical coupling, macro-scale models have been developed that describe both deformation and unsaturated flow. However, the constitutive relations in such models are still being debated; in particular the dependency of effective stress on capillary pressure and interfacial area, e.g. in Bishop's equation (*cf* Nikooee et al., 2013; Huyghe et al. 2017). In addition, macro-scale models entail many dependencies that must be identified prior to simulations. For example, hydraulic parameters such as (relative) permeability and capillary pressure-saturation curves depend on the state-of-stress of a porous material, which has been shown experimentally (see e.g. Nuth and Laloui, 2008; Salager et al., 2013; Oh and Lu, 2014; Tavakoli Dastjerdi et al., 2014) and numerically (see e.g. Rostami et al., 2015; Sweijen et al., 2016). Milatz and Grabe (2019) studied the relation of unsaturated flow with shearing of a grain-skeleton of sand, using CT imaging. Their study gave insight in the dependency of e.g. interfacial area of air and water on strain. For swelling materials, there are more constitutive equations required such as the effect of water saturation on the swelling rate and the effect

* Corresponding author.
E-mail address: S.M.Hassanizadeh@uu.nl (S.M. Hassanizadeh).

https://doi.org/10.1016/j.advwatres.2020.103642
Received 19 December 2019; Received in revised form 20 April 2020; Accepted 23 May 2020
Available online 31 May 2020

Table 1
Overview of simulations runs. The simulation number is also indicated in Fig. 4.

Simulation	Description	$k0$	τ_{abs}	τ_{def}	τ_{flow}
#1	Rigid packing	1	1	∞	1.33
#2	Swelling	0.1	10	9.2×10^{-5}	1.33
#3	Swelling	1	1	9.2×10^{-5}	1.33
#4	Swelling	10	0.1	9.2×10^{-5}	1.33
#5	No swelling	0	∞	9.2×10^{-5}	1.33

of swelling rate on water pressure inside the porous material (see e.g. Diersch et al., 2010).

Experimental characterization of swelling materials is complex, which is particularly true for swelling of SAP particles. The swelling and deformation are large and the period is short; typically, SAP absorbs 40 times its initial weight within 5 to 10 minutes (e.g. Kabiri et al., 2003).

An alternative to experiments would be to conduct pore-scale modelling based on pore-scale physics and rules. There is a huge literature on pore-network models for the description of (two-phase) flow and transport in granular porous media (see e.g., El-Zehairy et al., 2019; Molnar et al., 2019; Joekar-Niasar et al., 2010; Raoof and Hassanizadeh, 2010). In pore-network models, the pore space is explicitly reconstructed and one can account for pore sizes, shape, topology, and connectivity. Even possible changes of the pore space as a result of dissolution/precipitation (Wolterbeek and Raoof, 2018) or biofilm growth have been included (Qin and Hassanizadeh, 2015). However, in pore-network models, one cannot explicitly take into account the shape of grains, their movement and deformation, or temporal changes in shape and size.

A suitable grain-scale model for simulating deformation of particle packing's is the Discrete Element Method (DEM), which is capable of computing the movements of individual particles during deformation inside a 3-dimensional packing of particles (Cundall and Strack, 1979). DEM has previously been coupled to a pore network by Kharaghani et al. (2011) to study mechanical effects during drying. DEM can also be coupled with the Pore Finite Volume (PFV) method to simulate a number of different processes, such as: i) saturated flow inside deforming packings of spheres (Chareyre et al., 2012; Catalano et al., 2014); ii) fluidization of a bed of particles (Montellà et al., 2016), and iii) erosion of a particle bed (Hosn et al., 2019). DEM has also been coupled to the Pore-Unit Assembly (PUA) method, which subdivides the pore geometry into pore units and pore throats. Using the coupling of DEM with PUA, capillary pressure-saturation curves have been constructed for a large variety of particle packing's to study soil water retention curves (Yuan et al., 2015; Mahmoodlu et al., 2016; Sweijen et al., 2016). Thus, using DEM with either PFV or PUA allows for pore-scale simulations of the coupling between deformation and fluid flow (or capillarity). This yields insight into complex 3-dimensional processes of particle rearrangement and fluid flow inside granular materials, which otherwise would be difficult to study experimentally; see for example the comprehensive experimental work of MacMinn et al. (2015) on 2-dimensional particle rearrangement due to fluid flow.

Recently, Sweijen et al. (2018) coupled DEM to a pore-scale model for unsaturated flow. They developed a pore-scale model using IMPES (implicit pressure and explicit saturation scheme), which was based on PUA and could simulate dynamic drainage inside a rigid packing of spheres (thus not allowing for deformation). That work combines two-phase flow algorithms originating from pore-network models (see e.g., Thompson, 2002 and Joekar-Niasar et al., 2010) with the concept of pore-unit assembly. In the present work, the dynamic code of Sweijen et al. (2018) is extended to include large swelling of grains due to water absorption, their subsequent deformation, and the change of pore space. This is the first grain-scale model that is capable of simulating unsaturated flow in an packing of highly swelling grains.

The aim is to study swelling of a SAP particle bed and the subsequent drying (or drainage) of the pore space. To do so, we have the following objectives:

i) to develop a pore-scale model that can simulate unsaturated flow in deforming porous materials, by extending the coupling of DEM and PUA and include deformation;
ii) to identify processes that occur during drainage and swelling of SAP particle beds and to identify their characteristic time scales;
iii) to study a rigid packing of swelling particles;
iv) to study the effect of swelling rate of individual particles on the swelling behaviour a bed of particles.

These objectives are tested on a virtual particle bed of SAP particles inside a beaker glass. The packing is initially saturated with water. The SAP particles will start to swell and absorb water, whilst air will move into the particle packing from above. When the initial volume of water is absorbed, the particle packing will stop swelling.

2. Numerical methods

The simulation framework we use is the open-source software Yade, which is a 3-dimensional numerical model based on the Discrete Element Method, DEM (Šmilauer et al., 2015). In that framework, Sweijen et al. (2018) previously added the pore-unit assembly method to enable unsaturated flow inside particle packings. In this approach, an assembly of pore units is generated based on the particle locations in DEM. Using that assembly, unsaturated flow has been simulated for non-deforming assemblies of particles. In what follows, we extend the pore-unit assembly method to enable simulation of unsaturated flow and deformation, thus allowing for coupled calculations of unsaturated flow and particle movements following DEM. For simplification, in DEM calculations for determining the movement of grains, we do not include forces exerted on particles by pore fluids (air and/or water). The physical meaning of this assumption is that capillary and viscous forces, which act on particles, do not affect the movement of particles. In future work, adding forces that arise from the occupancy of pore units by water and water can relax this assumption, following the work byYuan and Chareyre, 2017 .

2.1. Determining the pore-unit assembly

In order to allow for coupling of DEM simulations with unsaturated flow, a meshing algorithm is employed that extracts a pore-unit assembly out of the particle configuration. Sweijen et al. (2018) introduced the meshing algorithm and a short summary is given here (see also Fig. 1). The lowest level of meshing is that of the particle centres, which is dependent on the state-of-stress inside the particle packing and which is determined by DEM. The particle centres determine the intermediate level of meshing, which is that of grain-based tetrahedra. Each grain-based tetrahedron has its vertices on the particle centres; this method relies on triangulation of the particle packing and was implemented into Yade by Chareyre et al. (2012) and Catalano et al. (2014). Each tetrahedron encloses a pore-space that is replaced by regular shape for sake of simplifying the pore geometry. When multiple tetrahedra enclose a single pore-space, the tetrahedra are merged and replaced by a different regular shape (see for more detail Sweijen et al., 2018). The assembly of regular shapes is the highest level of meshing, referred to as an assembly of pore units.

Regular shapes are for example tetrahedra, cubes, octahedra. Each regular shape is assumed to have its corners wedged into the pore throats of the particle packing. Since regular shapes have a known geometry, a library of geometrical constants are determined that describe the relation between capillary pressure (p_i^c) and saturation (s_i) within each pore-unit. The equation for p_i^c was initially defined by Joekar-Niasar et al. (2010) for cubical pore units and extended for various

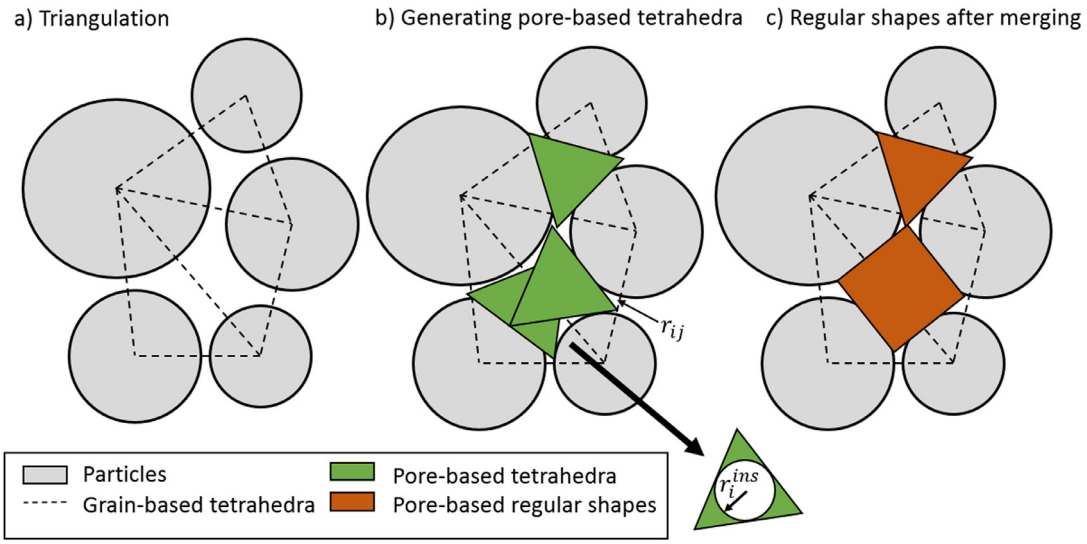

Fig. 1. Schematic overview of the meshing algorithm to abstract the pore-space inside a particle packing. Image from Sweijen et al. (2018).

shapes by Sweijen et al. (2018):

$$p_i^c = \frac{2\gamma}{\chi \sqrt[3]{V_i}(1 - e^{-\kappa s_i})} \quad (1)$$

where γ is the surface tension of air-water, χ and κ are geometrical constants, and V_i is the volume of a pore-unit.

In addition to the capillary pressure inside a pore unit, an entry criterium is imposed for air to invade a saturated pore unit *j* from a neighbouring pore unit *i*. the entry pressure of pore throat *ij* needs to be overcome. The entry criteria are implemented in Sweijen et al. (2018) and entails $p^{air} - p_j^w > \frac{2\gamma}{r_{ij}}$, with r_{ij} being the effective radius of pore throat *ij*.

Thus, the pore-unit assembly describes the connectivity of pore-units among each other, the size of pore units, the size of pore throats and the capillary pressure-saturation relations within each pore-unit. This assembly is then used to model unsaturated flow. To achieve hydro-mechanical coupling, changes in particle locations are directly projected to the grain-based tetrahedra and subsequently to the pore-unit assembly.

The numerical procedure contains the following three computational steps for every time step, see Fig. 2: i) update of particle locations, using DEM, ii) update of the local capillary pressure-saturation curve and pore throat entry pressures; iii) computation of unsaturated flow. Thus, first a time step is made by DEM to go from time t to time $t + \Delta t$, then flow computations are conducted to compute the water pressure and saturation at time $t + \Delta t$. In what follows, the algorithm to compute unsaturated flow is explained.

2.2. Change of pore-unit volume due to particle movement

Unsaturated flow is computed by an IMPES scheme (implicit pressure solver and an explicit saturation update as implemented into Yade by Sweijen et al., 2018).

Consider a pore unit i that has a volume V_i. The change in pore unit volume ($\frac{dV_i}{dt}$) is the sum of volume change due to swelling of the surrounding particles ($\frac{dV_i}{dt}|_{abs}$)and volume change due to the relative movement of particles ($\frac{dV_i}{dt}|_{mov}$), see Fig. 3. Thus, we have (following Sweijen et al., 2017b):

$$\frac{dV_i}{dt} = \frac{dV_i}{dt}\Big|_{mov} + \frac{dV_i}{dt}\Big|_{abs} \quad (2)$$

The value of $\frac{dV_i}{dt}|_{abs}$ is always negative during swelling and it is determined using the swelling rate of the enclosing particles which is further discussed in Section 3.1. Here, the change of particle volume, is assumed to be equal to the volume of absorbed water. As the mass density of swollen particles is almost the same as the water density, we can assume that the change in pore-unit volume due to water absorption by SAP particles is equal to the absorbed water volume. So, this change

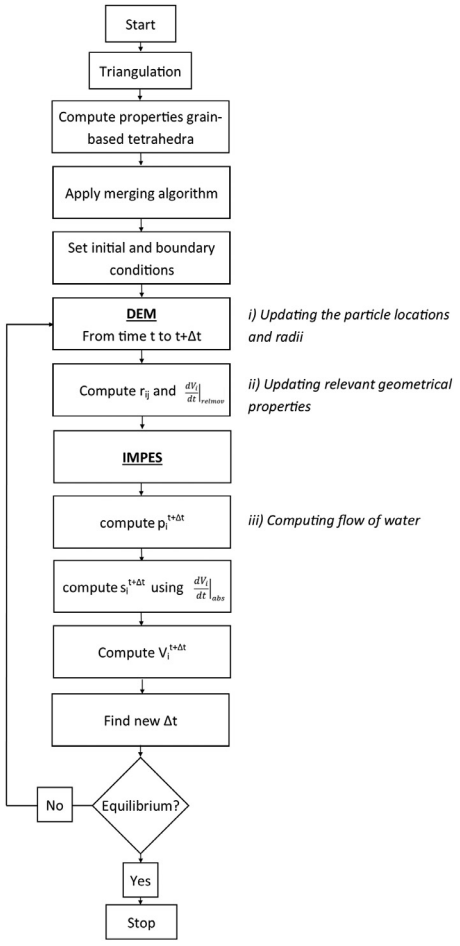

Fig. 2. Flowchart of the numerical scheme for coupling of the discrete element method with the pore-unit assembly method in order to simulate dynamic drainage in a deforming and swelling granular material.

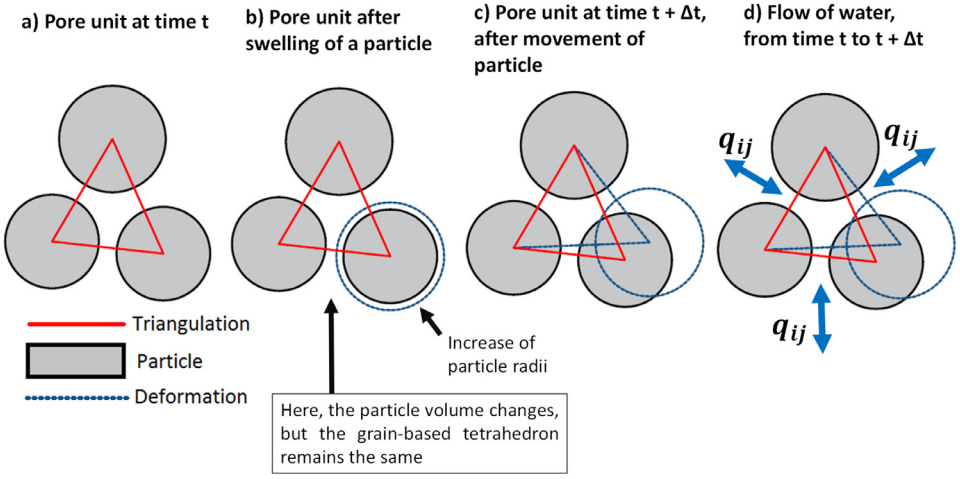

Fig. 3. 2-dimensional illustration of a deforming pore unit: a) the initial configuration, b) configuration after swelling of a particle, c) movement of particles due to deformation and d) flow of water as a result of particle motion, with *qij* being the volumetric flux in pore throat *ij*.

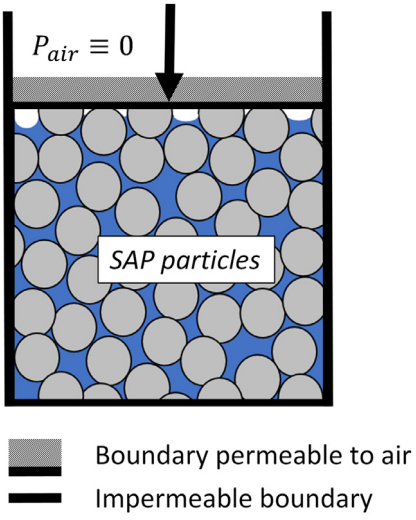

Fig. 4. 2-dimensional illustration of the boundary conditions that were used during swelling simulations. in our simulations.

does not directly cause flow of water, since water is simply changed from being in a liquid state to a solid state (i.e. absorbed into the SAP particle). But, a subsequent movement of particles will cause a change in void volume, which can cause movement of water. Therefore, the flux $\frac{dV_i}{dt}|_{mov}$ is considered when solving for pressure, while $\frac{dV_i}{dt}|_{abs}$ is only considered when updating the water saturation. The volume change terms in Eq. (1) are determined at time step $t + \Delta t$, based on the change in volume of the pore unit due to particle movement as well as swelling, using DEM.

2.3. Computation of unsaturated flow

In this section, the governing equations of flow in deforming pore units are provided. Consider pore unit i that has a water pressure p_i, a water saturation s_i and it is connected to neighbouring pore unit j via pore throat ij that has a conductivity k_{ij}. The volume balance for saturated pore units reads:

$$\sum_{j=1}^{N_i} k_{ij}(p_i - p_j) = -\frac{dV_i}{dt}\Big|_{mov} \tag{3}$$

Chareyre et al. (2012) and Catalano et al. (2014) have previously implemented Eq. 3 to solve for water pressure in saturated pore units in a deforming non-swelling granular material. For partially saturated pore units, the following discretized volume balance holds:

$$\sum_{j=1}^{N_i} k_{ij}\left({p_i}^{t+\Delta t} - {p_j}^{t+\Delta t}\right) = -\left(\frac{dV_i s_i}{dt}\Big|_{mov}\right)^{t+\Delta t} \tag{4}$$

Eq. 4 is non-linear as k_{ij} depends on the presence of air in pore units i and j as well as their capillary pressure (for more details see Sweijen et al., 2018). In addition, s_i depends on p_i contributing to the non-linearity of Eq. 4, therefore it requires simplifications before we can solve it for water pressure. The right-hand side of Eq. 4 is discretized into:

$$\left(\frac{dV_i s_i}{dt}\Big|_{mov}\right)^{t+\Delta t} = \frac{s_i^{t+\Delta t}V_i^{t+\Delta t} - s_i^t V_i^t}{\Delta t} \tag{5}$$

The value of $\frac{dV_i}{dt}|_{mov}$ is already known at time step $t + \Delta t$ from DEM computations, as explained above. Therefore, the term V_i^{t+t} is determined as follows:

$$V_i^{t+\Delta t} = V_i^t + \left(\frac{dV_i}{dt}\Big|_{mov}\right)^{t+\Delta t}\Delta t \tag{6}$$

Next, we introduce the following linearization to solve for saturation inside a pore unit:

$$s_i^{t+\Delta t} = s_i^t + \left(\frac{ds_i}{dp_i}\right)^t\left(\frac{dp_i}{dt}\right)^{t+\Delta t}\Delta t \tag{7}$$

where $\frac{ds_i}{dp_i}$ is the derivative of the local capillary pressure-saturation curve of each pore-unit (see Eq. 1). The value of $\frac{ds_i}{dp_i}$ is evaluated at time step t. After combining Eqs. 5 to 7, we have:

$$\left(\frac{dV_i s_i^w}{dt}\Big|_{mov}\right)^{t+\Delta t} = s_i^t\left(\frac{dV_i}{dt}\Big|_{mov}\right)^{t+\Delta t} + \left(V_i^t + \left(\frac{dV_i}{dt}\Big|_{mov}\right)^{t+\Delta t}\Delta t\right)\left(\frac{ds_i}{dp_i}\right)^t\left(\frac{dp_i}{dt}\right)^{t+\Delta t} \tag{8}$$

In Eq. 8, $(\frac{dp_i}{dt})^{t+\Delta t}$ can be rewritten as $\frac{p_i^{t+\Delta t} - p_i^t}{\Delta t}$. Combining Eqs. 4 and 8 and rearranging various terms yields:

$$p_i^{t+\Delta t}\left(\sum_{j=1}^{N_i} {k_{ij}}^t + \left[\frac{V_i^t}{\Delta t} + \left(\frac{dV_i}{dt}\Big|_{mov}\right)^{t+\Delta t}\right]\left(\frac{ds_i}{dp_i}\right)^t\right) - \sum_{j=1}^{N_i} {k_{ij}}^t {p_j}^{t+\Delta t} = -s_i^t\left(\frac{dV_i}{dt}\Big|_{mov}\right)^{t+\Delta t} + \left[\frac{V_i^t}{\Delta t} + \left(\frac{dV_i}{dt}\Big|_{mov}\right)^{t+\Delta t}\right]\frac{ds_i}{dp_i}\Big|^t p_i^t \tag{9}$$

Eqs. 4 and 9 constitute a set of linear equations that have the following form:

$$a{p_i}^{t+\Delta t} - \sum_{j=0}^{N_i} b{p_j}^{t+\Delta t} = c \tag{10}$$

where *a, b* and *c* are coefficients independent of p_i^{t+t}. Eq. 10 can be solved for water pressure. Note that the change of pore-unit volume due to particle movement, $\frac{dV_i}{dt}|_{mov}$ is obtained from DEM simulations. Eq. 10 simplifies into Eq. 1 for saturated pore units, which makes Eq. 10 applicable to saturated and unsaturated pore units. After obtaining p_i^{t+t}, the saturation is explicitly updated while accounting for the water absorption by the swelling particles:

$$s_i^{t+\Delta t} = s_i^t + \frac{ds_i}{dp_i}\left[\left(p_i^w\right)^{t+\Delta t} - \left(p_i^w\right)^t\right] + \frac{\Delta t}{V_i^{t+\Delta t}}\left.\frac{dV_i}{dt}\right|_{abs} \tag{11}$$

3. Model setup

3.1. Discrete Element Method setup

The Discrete Element Method was setup following previous work of the authors (Sweijen et al. 2017a) where the swelling behaviour of a saturated SAP particle bed was modelled and tested against experiments. In that work, the contact mechanics between the swelling particles is described by Hertz-Mindlin contact mechanics; see Modenese et al. (2012) for more details for its implementation. Contact mechanics in DEM are based on normal displacement between particles that results in a force, where the normal displacement is conceptualized as an "overlap" between two spherical particles. All particles were assumed to have a constant Young's modulus of 10 kPa. The particle-particle friction angle was set to 5.5° (Lorenz et al., 1997) and the density was set to 1000 kg•m^{-3} (Mirnyy et al., 2012). All particles had an initial diameter of 460μm.

Prior to swelling simulations, a packing of dry SAP particles was generated. First, 3000 particles were placed into a relatively large cubic modelling domain (10^3 mm^3). In such a relatively large domain, the particles do not form a tight packing and porosity is very large. Then, the particles were compacted by applying an artificial 10 Pa confining stress to all boundaries of the modelling domain, reducing the domain size significantly. This resulted in a porosity value of 0.38 and a domain size of 5.4^3 mm^3. The permeability of the dry SAP particle packing was determined using a virtual permeability test in Yade-DEM; the permeability was found to be 4.8×10^{-10} m^2. Once, a packing of dry SAP particles was generated, the boundary conditions were set to the conditions described in the following section.

After the particle packing was generated, the swelling simulations could commence. The swelling of particles was simulated by simply increasing all particle sizes over time, using a growth factor following Sweijen et al. (2017a). A simple kinetic law was used to describe the change of radius as a function of time, although more complex and comprehensive models exist for swelling of spherical particle (Huyghe and Jansen, 1997; Radu et al., 2002; Sweijen et al., 2017b). Here, we employed the kinetic law proposed by Omidian et al. (1998) with an additional factor to account for partial wetting of the particle surface under unsaturated conditions (following Diersch et al., 2010):

$$\frac{dR_x}{dt} = f_w k^0\left(R_x^{max} - R_x\right) \tag{12}$$

where k^0 is a kinetic coefficient, f_w is the fraction of the wetted surface of a particle R_x is the radius, R_{max} is the maximum radius. The fraction f_w is the ratio of the surface area of particle x that is in contact with water and the total surface area of particle x. The maximum radius was set to $3.6R_0$, where R_0 was the initial radius; this corresponded to an absorption ratio of 30 g/g. Furthermore, the swelling rate is expressed as a dimensionless group: $\frac{1}{(k^0 R^0)}\frac{dR}{dt}$, where R is the arithmetic mean of radii of all particle.

Eq. 12 plays an important role in the coupling of DEM with the model for unsaturated flow. If a particle is surrounded by empty pores, its swelling rate converges to zero. If a particle is only surrounded by fully saturated pore units, its swelling rate is at a maximum value but still dependent on its radius and initial radius. The wetted surface area of a particle is based on the saturation of the surrounding pore units. If a pore unit is empty (saturation lower than 10^{-6}), the solid surface area in that pore unit is dry otherwise it is considered wet.

3.2. Initial and boundary conditions

In this study, we simulate a one-direction swelling experiment in a box similar to swelling of particles in a beaker glass. The side walls and the bottom of the box are fixed and the top boundary is free to move (see Figure 4). All boundaries are no-flow boundary conditions to water and only via the top boundary air can enter into the particle packing. We assume that at the start of the experiment, the bed of SAP particles becomes saturated quickly, without any significant swelling. As a result the particle bed is fully saturated, except for the pore units along the top boundary, which are partially saturated with air at an initial capillary pressure of 2500 Pa.

The initial volume of water inside the pores in between the particles is the only available water for swelling throughout the simulation. Note that SAP particles are considered non-porous themselves and thus initially do not contain any water. After the initial conditions, the particles start to absorb water and swell and the particle packing will increase in height. Eventually the particle bed dries out and swelling will cease.

3.3. Different regimes in the coupling of unsaturated flow, swelling and particle movement

Three different processes govern unsaturated flow inside the pore space of a swelling particle bed, with each process having its own characteristic time step, namely: unsaturated flow (τ_{flow}), water absorption (τ_{abs}), and deformation (τ_{def}). The magnitude of the characteristic times will give insight into the behaviour of the particle packing. Therefore, we introduce the characteristic times and their effect on the overall swelling behaviour of a bed of particles.

The characteristic time of water absorption (τ_{abs}) is based on Eq. 12 such that:

$$\tau_{abs} = \frac{\left(R_i^{max} - R_i\right)}{\frac{dR_i}{dt}} = \frac{1}{f_w k^0} \tag{13}$$

Now, if we define f_w to be the fraction of wetted surface of all particles in the packing, then the second part of Eq. 13 is used to determine characteristic time for swelling of the whole particle packing. The characteristic time for unsaturated flow (τ_{flow}) is given as:

$$\tau_{flow} = \frac{l}{v} = \frac{l\mu}{\rho_w g K} = \frac{\mu dx}{K dP} \tag{14}$$

where μ is the viscosity of water, l is the length of the modelling domain, ρ_w is the density of water, g is the gravitational constant, q is the Darcy flux, K is the intrinsic permeability of the modelling domain and $\frac{dP}{dx}$ is the pressure gradient in water. Finally, we introduce the time scale for deformation, which is based on the relaxation time required for a contact to dissipate its potential energy:

$$\tau_{def} = \frac{\bar{R}}{2}\sqrt{\frac{\rho}{E}} \tag{15}$$

in which E is the Young's modulus of the particles, ρ is the particle density (assumed to be 1 g cm^{-3}) and $\bar{R}$ is the average particle diameter.

To illustrate the effect of three characteristic times on the overall swelling behaviour, we define the following ratios of time scales:

$$\frac{\tau_{flow}}{\tau_{abs}} = \frac{l\mu f_w k^0}{\rho_w g K} \approx 1.15[s]\ f_w k^0 \tag{16}$$

$$\frac{\tau_{def}}{\tau_{abs}} = \frac{D_{50} f_w k^0}{2}\sqrt{\frac{\rho}{E}} \approx 7.3 \times 10^{-5}[s]\ f_w k^0 \tag{17}$$

$$\frac{\tau_{flow}}{\tau_{def}} = \frac{2l\mu}{\rho_w g K D_{50}\sqrt{\frac{\rho}{E}}} \approx 1.6 \times 10^4 \tag{18}$$

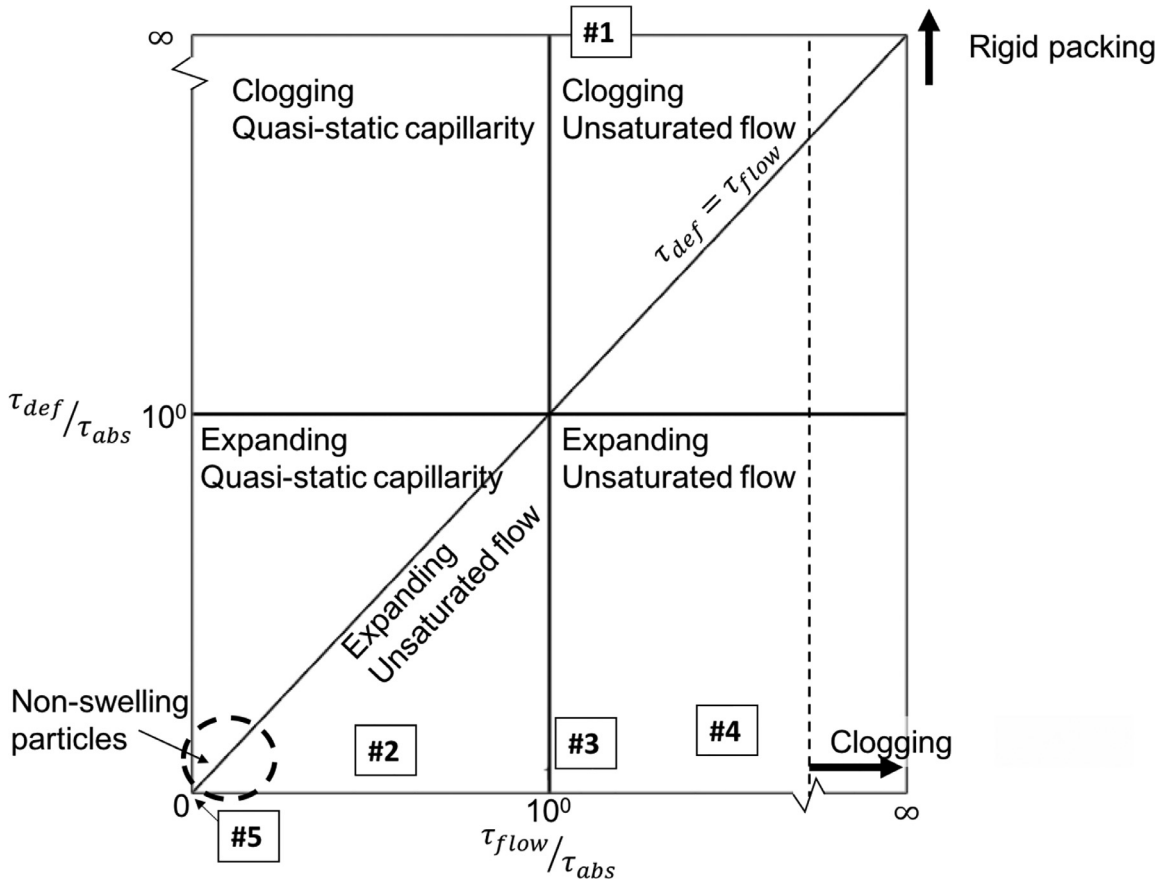

Fig. 5. Overview of time-scales of deformation, absorption kinetics, and flow. Indicated are the type of modelling approaches that can be employed depending on the characteristic time steps. The particle packing can be expanding or rigid (i.e. clogging occurs) whereas flow can be much faster than deformation (quasi-static capillarity) or have a similar time scale as deformation (unsaturated flow).

Using Eqs. 16–18, we can identify the following cases (which are also illustrated in Fig. 5):

i) $\tau_{flow} \ll \tau_{abs}$, water residing inside the pores can find equilibrium very fast and thus dynamic effects of unsaturated flow will be short-lived. Therefore, unsaturated flow can be simulated using a quasi-static capillarity model rather than a dynamic code.
ii) $\tau_{flow} \gg \tau_{abs}$, water exchange among pores is slow and thus the swelling rate may be strongly affected by the lack of water inside the particle packing, which might cause suction inside the particle packing even when it is saturated.
iii) $\tau_{def} \ll \tau_{abs}$, the particle-particle contact points can dissipate their potential energy quickly. In practise, τ_{def} is always smaller than τ_{abs} and thus particle movement can keep up with the deformation.
iv) $\tau_{def} \gg \tau_{abs}$, swelling is much faster than that particle contacts can dissipate their potential energy. Therefore, particle movement will be limited and the particle packing will clog (i.e. the porosity will tend to zero). This scenario will be similar to swelling of a bed of particles inside a rigid box, where particle movement will also be restricted.
v) $\tau_{flow} \ll \tau_{def}$, water residing inside the pores can find equilibrium very fast and thus dynamic effects will be short-lived.
vi) $\tau_{flow} \gg \tau_{def}$, particle contacts can dissipate their energy quickly and thus the flow of water will be dominating the kinetics of particle movement.

For swelling SAP particles, we have $\frac{\tau_{flow}}{\tau_{def}} > 1$ and $\frac{\tau_{def}}{\tau_{abs}} < 1$, indicating that the relaxation of particle contacts occurs fast compared to flow and water absorption processes. Nevertheless, we consider one scenario, simulation #1, where particles are not allowed to move (*i.e.*, $\tau_{def} \to \infty$). In addition, we conduct three simulations for varying values of k^0 starting from 0.1 to 10 s^{-1} (simulation #2 to #4), which varies $\frac{\tau_{flow}}{\tau_{abs}}$ from 0.115 to 11.5. Thus the value of $\frac{\tau_{flow}}{\tau_{abs}}$ at the initial state of swelling is around unity, which implicates that swelling and unsaturated flow have similar time scales. Lastly, we consider a hypothetical packing where no swelling occurs, i.e., $\tau_{abs} \to \infty$ (simulation #5), and thus nothing happens because particle locations do not change and all pores remain saturated. The characteristic times steps are summarize in Table 1.

In practise, the value of $\frac{\tau_{flow}}{\tau_{abs}}$ is in the order of 10, based on the experimental work by Mirnyy et al. (2013) where we have $k^0 = 5 \bullet 10^{-3} s^{-1}$, $l = 0.20\, m$ (Mirnyy et al. 2013), $K = 10^{-11} m^2$ (Diersch et al. 2011). This implies that the experimental work by Mirnyy et al. (2013) is best represented by simulation #4, which has $\frac{\tau_{flow}}{\tau_{abs}}$ equal to 11.5.

3.4. Mechanical considerations

As mentioned earlier, we made some assumptions regarding the mechanics of particles and the packing. First, forces on the particles exerted by the surrounding fluids (i.e. air and/or water) were not included. As the water pressure in the packing would be smaller than the air pressure, the particle packing would in experiments be more compressed by the suction of water. Secondly, the particles are assumed to keep their initial spherical shape during swelling, thus particles cannot grow into available pore-space, which implies that case iv of section 3.3 cannot be modelled using our code. In real SAP particle packings, we may have

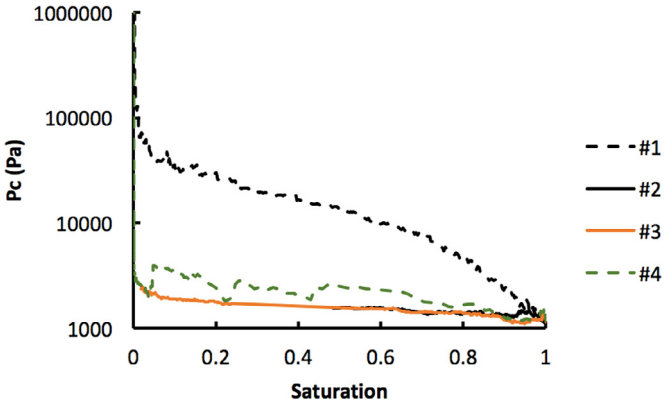

Fig. 6. Capillary pressure-saturation curves for simulations #1 to #4.

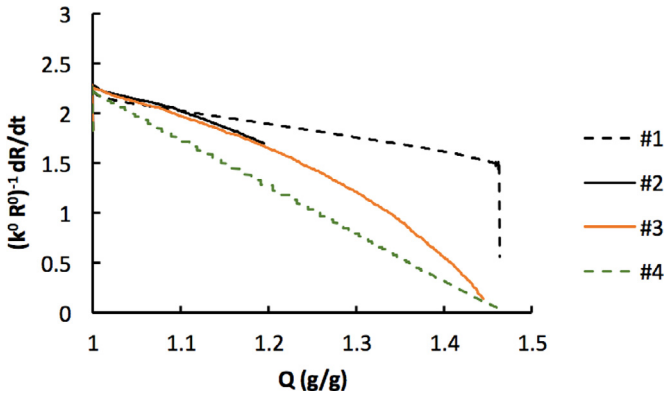

Fig. 7. The normalized and averaged particle swelling rate as a function of average absorption ratio for simulations #1 to #4.

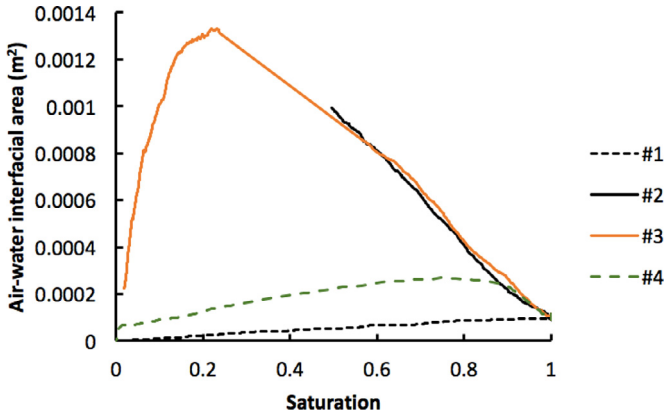

Fig. 8. The air-water interfacial area as a function of saturation for simulations #1 to #4.

plastic deformation of particles and a change of their shape whilst our code assumes that normal displacement at particle contacts is purely a reversible deformation.

3.5. Mass balance of the simulations

The coupling of unsaturated flow with DEM requires two mass-balances in order to verify the quality of the numerical simulations. Firstly, modelling of unsaturated flow requires a mass-balance on its own for solving Eqs. 10 and 11. The mass-balance is verified at each time step and the accumulative error is registered over time. From these analysis it follows that locally at each time step mass is conserved, with the inclusion of very small truncation loss of saturation (at saturations of lower than 10^{-6}). The accumulative error is largest for simulation #1 with 0.2%, which was a result of the rigid packing in which porosity tends to zero.

Secondly there is a mass balance of the coupling between unsaturated flow and DEM, which is mostly affected by the normal-displacement at particle contacts, the larger the normal displacement, the larger the error in mass-balance becomes. Thus with larger values of $\frac{\tau_{flow}}{\tau_{abs}}$, the error increases from an accumulative error in water balance from 1% (simulation #2) to 8% (simulation #4).

4. Results and discussion

4.1. The swelling of a rigid packing

In simulation #1, the particle locations are fixed in order to study the swelling of a rigid packing. This scenario is purely hypothetical, but would be similar to swelling particles inside a rigid box. In theory, the saturation inside the particle packing should remain equal to unity as water inside the pore space is simply transferred to the solid phase; i.e. particles swell into the available pore space and the porosity will converge to zero. Since DEM does not allow for the change of shape of spherical particles, the numerical model cannot simulate a particle packing whose porosity value converges to zero and consequently DEM overestimates the normal displacement at contact points and thus too much particle volume "overlaps". As a result, water suction arises inside the particle packing causing an increase in capillary pressure. Even though the results of simulation #1 are purely hypothetical, we use results of simulation #1 to gain insight and compare to other cases.

Fig. 6 shows the capillary pressure-saturation curve for simulation #1, which has substantially larger values of capillary pressure compared to other simulations for expanding domains due to the decrease in pore throat and pore unit radii with swelling. As seen in Fig. 7, the swelling rate decreases linearly with the amount of absorption. Its value is larger than the other simulations because the majority of the pore units remain water saturated, while in scenarios #2 to #4 air is invading and thus reducing the wetted surface area of grains.

4.2. The effect of swelling rate

To study the effect of swelling rate, we varied the value of k^0 from 0.10 to 10 s^{-1} in simulations #2 to #4. Figure 6 shows that the capillary pressure values are increasing with k^0, thus with $\frac{\tau_{flow}}{\tau_{abs}}$ (note that $\frac{\tau_{def}}{\tau_{abs}}$ remains very small with increasing k^0). For simulations #2 and #3, $\frac{\tau_{flow}}{\tau_{abs}}$ is small enough for the distribution of water and air to be close-to-equilibrium during swelling of the particles. But, for simulation #4, the swelling rate becomes too large compared to the speed at which air is able to move into the particle packing causing a significant water suction gradient inside the packing. In other words, air-water interfaces do not move easily into the particle packing when swelling is fast. Consequently, the capillary pressure increases and the air-water interfacial area is lower than that for slow swelling simulations (#2 and #3). Thus, simulation #4 results in lower values of air-water interfacial area than for simulations #2 and #3, as shown in Fig. 8 and 9. In addition, the fast swelling rate in simulation #4 prevents air from infiltrating at low absorption ratios and, therefore, the saturation decreases less with absorption ratio than simulations #2 and #3 (see Fig. 8). As a consequence, the swelling rate decreases at higher values of absorption ratio for simulation #4 than those of #2 and #3; see Fig. 7.

The swelling rate also affects the evolution of the height of the particle bed; see Fig. 10. If $\frac{\tau_{flow}}{\tau_{abs}}$ is small enough for unsaturated flow to sustain the swelling rate (simulations #2 and #3), then the general observation is: the higher the swelling rate, the less efficient the particle

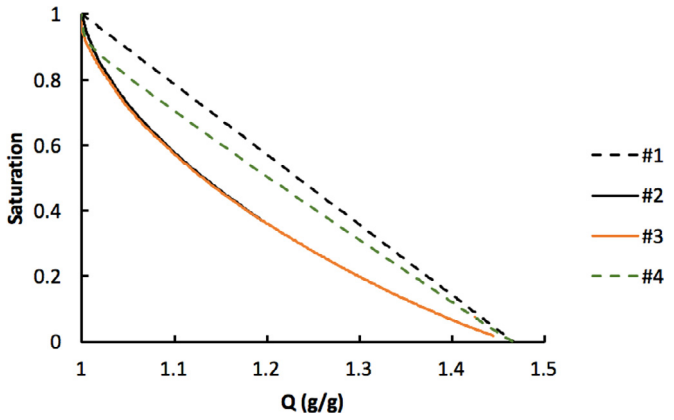

Fig. 9. Saturation as a function of absorption ratio for simulations #1 to #4.

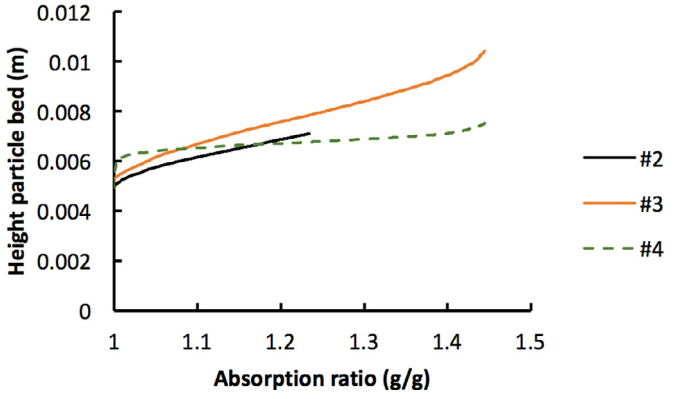

Fig. 10. The height of the particle bed as a function of absorption ratio.

packing deforms. Consequently, the particle packing has a higher porosity value and a taller particle bed. For the first part of swelling, this observation also applies to simulation #4 as it has a higher swelling rate than simulations #2 and #3 and thus the particle bed is taller than the other samples. However, air-water interfaces are not developed in the particle packing for simulation #4 and thus the expansion of the particle bed ceases.

4.3. Solid-water interfacial area as function of swelling and saturation

In the continuum-scale model developed by Diersch et al. (2010), the following equation was employed to approximate the wetted fraction particles surface area as a function of saturation (S):

$$f_w = \frac{1-e^{-S\alpha_{exp}}}{1-e^{-\alpha_{exp}}} \tag{22}$$

where α_{exp} is a fitting parameter. The values of f_w for different saturation values as calculated in simulations #2 and #3 are plotted in Fig. 11 and can be fitted using Eq. (22) with $\alpha_{exp} = 4.1$, while data of simulation #4 can be fitted with $\alpha_{exp} = 0.85$.

Mirnyy et al. (2013) reported also a positive value of α_{exp}, namely 0.4 based on backfitting of their model on experiments. To enable a comparison between the work by Mirnyy et al. (2013) and our simulations, we employ the value of $\frac{\tau_{flow}}{\tau_{abs}}$ to evaluate α_{exp}. From Section 3.3 it appears that simulation #4 has a similar value of $\frac{\tau_{flow}}{\tau_{abs}}$ to the experimental data by Mirnyy et al. (2013). Our numerical results show that simulation #4 has a similar $f_w(s)$ curve as that of Mirnyy et al. (2013), and therefore the value for α_{exp}.between Mirnyy et al. (2013) and our simulations is similar, namely 0.40 and 0,85 respectively.

To conclude, the fraction f_w not only depends on saturation S but also on the flow rate compared to the swelling rate (i.e. $\frac{\tau_{flow}}{\tau_{abs}}$) because

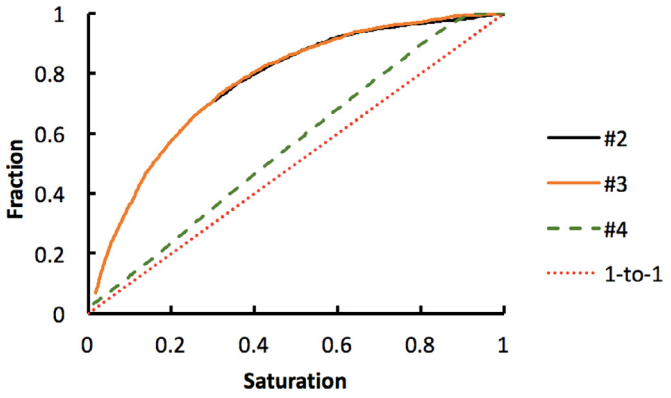

Fig. 11. The fraction of wetted solid area, normalized to the total solid area as a function of saturation for simulations #2 to #4 as well as a 1-to-1 ratio line (dashed red line).(For interpretation of the references to color in this figure legend, the reader is referred to the web version of this article.)

scenario's #2 and #3 yield the same $f_w(S)$ relation, but simulation #4 gives a different relation that yields lower values for f_w.

5. Conclusions

We have developed a grain-scale modelling technique for the simulation of unsaturated flow in deforming and highly swelling granular materials. The discrete element method was used for calculations of swelling and the subsequent deformation of particle packings. Unsaturated flow was solved using a pore-scale model, using IMPES (implicit pressure and explicit saturation scheme) that was tailored for pore units in a deforming packing of spheres. Deformation was included by changing the volume of pore units, pore unit radii, pore throat radii during swelling. Simulations were conducted for swelling of a bed of particles that absorbs one pore volume of water. Results indicated that by varying the swelling coefficient swelling behaviour is substantially affected. If unsaturated flow is sufficiently fast, the water pressure remains close to hydrostatic conditions while if unsaturated flow is slow, a water suction arises inside the particle packing as a consequent of the swelling. Furthermore, we show that the fraction of wetted solid surface area as a function of saturation is not a unique function, and it depends on the ratio of the time scales of flow τ_{flow} and absorption τ_{abs}, thus on $\frac{\tau_{flow}}{\tau_{abs}}$.

Declaration of Competing Interest

None.

CRediT authorship contribution statement

Thomas Sweijen: Conceptualization, Methodology, Software, Writing - original draft, Visualization. **S. Majid Hassanizadeh:** Conceptualization, Writing - review & editing, Supervision, Funding acquisition. **Bruno Chareyre:** Conceptualization, Methodology, Software, Writing - review & editing.

Acknowledgements

The first author gratefully acknowledges financial support from the Technology Foundation STW, the technological branch of the Netherlands Organization of Scientific Research, NWO, and the Dutch ministry of Economic Affairs under contract no. 12538, entitled Interfacial effects in ionized media. The second author would like to thank European Research Council for supporting this research under the European Union's Seventh Framework Programme (FP/2007-2013)/ERC Grant Agreement no. 341225. The third author acknowledges the CRCT granted by Grenoble INP in 2012 which allowed this joint research. All

authors gratefully acknowledge the Van Gogh Program 2016 under no. 35530VM. We gratefully acknowledge the valuable comments by Stefan Luding.

Supplementary materials

Supplementary material associated with this article can be found, in the online version, at doi:10.1016/j.advwatres.2020.103642.

References

Bertrand, T., Peixinho, J., Mukhopadhyay, S., MacMinn, C.W., 2016. Dynamics of swelling and drying in a spherical gel. Phys. Rev. Appl. 6 (6), 064010.

Catalano, E., Chareyre, B., Barthélémy, E., 2014. Pore-scale modeling of fluid-particles interaction and emerging poromechanical effects. Int. J. Numer. Anal. Methods Geomech. 38 (1), 51–71.

Chareyre, B., Cortis, A., Catalano, E., Barthélemy, E., 2012. Pore-scale modeling of viscous flow and induced forces in dense sphere packings. Transp. Porous Media 94 (2), 595–615.

Cundall, P.A., Strack, O.D., 1979. A discrete numerical model for granular assemblies. Geotechnique 29 (1), 47–65.

... Diersch, H.G., Clausnitzer, V., Myrnyy, V., Rosati, R., Schmidt, M., Beruda, H., Virgilio, R., 2010. Modeling unsaturated flow in absorbent swelling porous media: Part 1. theory. Transp. Porous Media 83 (3), 437–464.

... Diersch, H.G., Clausnitzer, V., Myrnyy, V., Rosati, R., Schmidt, M., Beruda, H., Virgilio, R., 2011. Modeling unsaturated flow in absorbent swelling porous media: Part 2. Numerical simulation. Transp. Porous Media 86, 753–776.

Ding, J., Remmers, J.J., Leszczynski, S., Huyghe, J.M., 2018. Swelling driven crack propagation in large deformation in ionized hydrogel. J. Appl. Mech. 85 (2), 021007.

El-Zehairy, Mousavi Nezhad M., Joekar-Niasar V., Guymer I., Kourra N., William M. A. (2019) Pore-network modelling of non-Darcy flow through heterogeneous porous media; Adv. Water Res.131 (2019) 103378

Espinoza, D., Vandamme, M., Pereira, J., Dangla, P., Vidal-Gilbert, S., 2014. Measurement and modeling of adsorptive–poromechanical properties of bituminous coal cores exposed to CO_2: Adsorption, swelling strains, swelling stresses and impact on fracture permeability. Int. J. Coal Geol. 134, 80–95.

Graham, A.T., Wilson, L.R., 1998. Commercial processes for the manufacture of superabsorbent polymers. In: Buchholz, F.L., Graham, A.T. (Eds.), Modern Superabsorbent Polymer Technology. John Wiley & Sons, Inc, pp. 69–118.

Huyghe, J.M., Janssen, J., 1997. Quadriphasic mechanics of swelling incompressible porous media. Int. J. Eng. Sci. 35 (8), 793–802.

Huyghe, J., Nikooee, E., Hassanizadeh, S., 2017. Bridging effective stress and soil water retention equations in deforming unsaturated porous media: a thermodynamic approach. Transp. Porous Media 117 (3), 349–365.

Joekar-Niasar, V., Hassanizadeh, S.M., Dahle, H., 2010. Non-equilibrium effects in capillarity and interfacial area in two-phase flow: dynamic pore-network modelling. J. Fluid Mech. 655, 38–71.

Kabiri, K., Omidian, H., Hashemi, S., Zohuriaan-Mehr, M., 2003. Synthesis of fast-swelling superabsorbent hydrogels: effect of crosslinker type and concentration on porosity and absorption rate. Eur. Polym. J. 39 (7), 1341–1348.

Lamminmäki, T., Kettle, J., Puukko, P., Ridgway, C., Gane, P., 2012. Short timescale inkjet ink component diffusion: an active part of the absorption mechanism into inkjet coatings. J. Colloid Interface Sci. 365 (1), 222–235.

Lorenz, A., Tuozzolo, C., Louge, M., 1997. Measurements of impact properties of small, nearly spherical particles. Exp. Mech. 37 (3), 292–298.

MacMinn, C.W., Dufresne, E.R., Wettlaufer, J.S., 2015. Fluid-driven deformation of a soft granular material. Phys. Rev. X 5 (1), 011020.

Mahmoodlu, M.G., Raoof, A., Sweijen, T., van Genuchten, M.T., 2016. Effects of sand compaction and mixing on pore structure and the unsaturated soil hydraulic properties. Vadose Zone J. 15 (8).

Mirnyy, V., Clausnitzer, V., Diersch, H.G., Rosati, R., Schmidt, M., Beruda, H., 2012. Wicking in absorbent swelling porous materials. In: Wicking in Porous Materials: Traditional and Modern Modeling Approaches, pp. 161–200.

Modenese, C., Utili, S., Houlsby, G., 2012. DEM modelling of elastic adhesive particles with application to lunar soil. Earth Space 1, 45–54.

Molnar, I.L., Gerhard, J.I., Willson, C.S., O'Carrol, D.M., 2019. Wettability effects on primary drainage mechanisms and NAP distribution: a pore-scale study. Water Resour. Res. (Accepted).

Milatz, M., Grabe, J. (2019). Microscopic investigation of the hydro-mechanical behaviour of unsaturated granular media with X-ray CT. Japanese Geotechnical Society Special Publication 7.2 (2019): 615-626

Montellà, E., Toraldo, M., Chareyre, B., Sibille, L., 2016. Localized fluidization in granular materials: theoretical and numerical study. Phys. Rev. E 94 (5), 052905.

Nikooee, E., Habibagahi, G., Hassanizadeh, S.M., Ghahramani, A., 2013. Effective stress in unsaturated soils: a thermodynamic approach based on the interfacial energy and hydromechanical coupling. Transp. Porous Media 96 (2), 369–396.

Nuth, M., Laloui, L., 2008. Advances in modelling hysteretic water retention curve in deformable soils. Comput. Geotech. 35 (6), 835–844.

Oh, S., Lu, N., 2014. Uniqueness of the suction stress characteristic curve under different confining stress conditions. Vadose Zone J. 13 (5).

Omidian, H., Hashemi, S., Sammes, P., Meldrum, I., 1998. A model for the swelling of superabsorbent polymers. Polymer 39 (26), 6697–6704.

Pan, Z., Connell, L.D., 2012. Modelling permeability for coal reservoirs: a review of analytical models and testing data. Int. J. Coal Geol. 92, 1–44.

Qin, C., Hassanizadeh, S.M., 2015. Pore-network modeling of solute transport and biofilm growth in porous media. Transp. Porous Med. 110, 345–367 2015.

Radu, F.A., Bause, M., Knabner, P., Lee, G.W., Friess, W.C., 2002. Modeling of drug release from collagen matrices. J. Pharm. Sci. 91 (4), 964–972.

Raoof, A., Hassanizadeh, S.M., 2010. A new method for generating pore-network models of porous media. Transp. Porous Media 81 (3), 391–407.

Rostami, A., Habibagahi, G., Ajdari, M., Nikooee, E., 2015. Pore network investigation on hysteresis phenomena and influence of stress state on the SWRC. Int. J. Geomech. 15 (5), 04014072.

Salager, S., Nuth, M., Ferrari, A., Laloui, L., 2013. Investigation into water retention behaviour of deformable soils. Can. Geotech. J. 50 (2), 200–208.

Sweijen, T., Chareyre, B., Hassanizadeh, S., Karadimitriou, N., 2017. Grain-scale modelling of swelling granular materials; application to super absorbent polymers. Powder Technol..

Sweijen, T., van Duijn, C., Hassanizadeh, S., 2017. A model for diffusion of water into a swelling particle with a free boundary: application to a super absorbent polymer particle. Chem. Eng. Sci..

Sweijen, T., Hassanizadeh, S.M., Chareyre, B., Zhuang, L., 2018. A dynamic pore-scale model of drainage in granular porous media: the pore-unit assembly method. Adv.Water Resour. (UNDER REVIEW).

Sweijen, T., Nikooee, E., Hassanizadeh, S.M., Chareyre, B., 2016. The effects of swelling and porosity change on capillarity: DEM coupled with a pore-unit assembly method. Transp. Porous Media 113 (1), 207–226.

Takhar, P.S., 2014. Unsaturated fluid transport in swelling poroviscoelastic biopolymers. Chem. Eng. Sci. 109, 98–110.

Dastjerdi, Tavakoli, H., M., Habibagahi, G., Nikooee, E., 2014. Effect of confining stress on soil water retention curve and its impact on the shear strength of unsaturated soils. Vadose Zone J. 13 (5).

Tester, R.F., Morrison, W.R., 1990. Swelling and gelatinization of cereal starches. II. waxy rice starches. Cereal. Chem. 67 (6), 558–563.

Thompson, K.E., 2002. Pore-scale modeling of fluid transport in disordered fibrous materials. AIChE J. 48 (7), 1369–1389.

Wolterbeek, T.K.T., Raoof, A., 2018. Meter-scale reactive transport modeling of CO_2-rich fluid flow along debonden wellbore casing-cement interfaces. Environ. Sci. Technol. 52, 3786–3795 2018.

Yeh, A., Li, J., 1996. A continuous measurement of swelling of rice starch during heating. J. Cereal Sci. 23 (3), 277–283.

Yu, C., Malakpoor, K., Leszczynski, S., & Huyghe, J. A full 3D mixed hybrid finite element model of superabsorbent polymers. Poromechanics VI (pp. 362-369)

Yuan, C., Chareyre, B., 2017. A pore-scale method for hydromechanical coupling in deformable granular media. Comput. Meth. Appl. Mech. Eng. 318, 1066–1079.

Yuan, C., Chareyre, B., Darve, F., 2015. Pore-scale simulations of drainage in granular materials: Finite size effects and the representative elementary volume. Adv. Water Resour..